An Analytical Hybrid GORT Model for Bidirectional Reflectance Over Discontinuous Plant Canopies

Wenge Ni, *Member, IEEE,* Xiaowen Li, Curtis E. Woodcock, *Member, IEEE,*
Mário R. Caetano, and Alan H. Strahler, *Member, IEEE*

***Abstract*—The geometric optical (GO) bidirectional reflectance model, combined with a new component spectral signature submodel, can be used to estimate the bidirectional reflectance distribution function (BRDF) of discontinuous canopies. This approach retains the GO approach of incorporating the effect of shadows cast by crowns on the background. The newly developed submodel uses an analytical approximation of the radiative transfer (RT) within the plant canopies to model the spectral properties of each scene component. A multiple scale-hotspot function that incorporates effects for smaller canopy objects like branches, stems and leaves was also well modeled. Comparison of model results with field measurements (ASAS, POLDER and PARABOLA) over an old black spruce forest in central Canada demonstrated that the model can predict the basic features of the BRDF, i.e., bowl shape and the hotspot. The benefits of the model presented are simplicity, improved treatment of multiple scattering and a new method of estimating the component signatures.**

***Index Terms*— Analytical GORT-BRDF model, discontinuous plant canopies.**

NOMENCLATURE

Roman:

$B(\theta_i, \theta_v, \phi)$	Hotspot function.
$C(\theta_i, \theta_v)$	Signature of sunlit crown surface.
D	Crown diameter.
f_d	Beam proportion.
FAVD	Foliage area volume density.
G	Signature of sunlit background.
g	Phase function asymmetry factor
$H(n>0\|h, \theta_i, \theta_v, \phi)$	Hotspot correction factor at incident zenith angle θ_i and viewing zenith angle θ_v at depth h. For the whole canopy, it is written as $H(n>0\|\theta_i, \theta_v, \phi)$.
h	Depth of canopy layer.
$k(\theta_i)$	Leaf orientation factor.
$K_{open}(n=0)$	Between-crown openness factor.
$K_{open}(n>0)$	Within-crown openness factor.
$K_c(\theta_i, \theta_v \phi)$	Areal proportion of sunlit and viewed crown surface.
$K_g(\theta_i, \theta_v \phi)$	Areal proportion of sunlit and viewed background.
$K'_g(\theta_i, \theta_v \phi)$	Areal proportion of sunlit and nonviewable ground surface.
$K_t(\theta_i, \theta_v \phi)$	Areal proportion of shaded and viewed crown surface.
$K_z(\theta_i, \theta_v \phi)$	Areal proportion of shaded and viewed background.
$K'_z(\theta_i, \theta_v \phi)$	Areal proportion of shaded and nonviewable background.
$l_i(\theta_v)$	Within-crown path length within a single crown at viewing zenith angle θ_v.
$l_v(\theta_i)$	Within-crown path length within a single crown at incident zenith angle θ_i.
$l_{i,v}(\theta_i, \theta_v)$	$= \sqrt{l_i^2 + l_v^2 - 2 l_i l_v \cos\xi}$.
L_e	Effective leaf area index $(m^2 m^{-2})$.
$P(n=0\|h, \theta_i)$	Between-crown gap probability for a beam at θ_i at depth h for the whole canopy; it is written as $P(n=0\|\theta_i)$.
$P(n>0\|h, \theta_i)$	Within-crown gap probability for a beam at θ_i at depth h for the whole canopy, it is written as $P(n>0\|\theta_i)$.
$P(n>0\|h, \theta_i, \theta_v, \phi)$	Bidirectional within-crown gap probability at incident zenith angle θ_i and viewing zenith angle θ_v and at depth h. For the whole canopy, it is written as $P(n>0\|\theta_i, \theta_v, \phi)$.
R^{∞}_{df}	Directional hemispherical path reflectance for a semi-infinite horizontally homogeneous medium with incident angle θ_i.
R^{∞}_{ff}	Hemispherical hemispherical path reflectance of a semi-infinite horizontally homogeneous medium.
$R(\theta_i, \theta_v)$	Bidirectional reflectance factor.
r	Horizontal crown radius (m).
r_L	Leaf reflectance.
s_l	Characteristic linear dimension of foliage elements.

Manuscript received January 12, 1998; revised August 25, 1998. This work was supported in part by U.S. Army Corps of Engineering under Contract DACA89-93-k-00012; by NASA under Contract NAS5-31369, and by China's "National Key-Importance Basic Research Plan."

W. Ni is with the Department of Geography and Center for Remote Sensing, Boston University, Boston, MA, 02215 USA. She is also with Raytheon STX, Lanham, MD 20706 USA (e-mail: ni@homer.stx.com).

C. E. Woodcock, and A. H. Strahler are with the Department of Geography and Center for Remote Sensing, Boston University, Boston, MA, 02215 USA.

X. Li is with the Department of Geography and Center for Remote Sensing, Boston University, Boston, MA, 02215 USA, and with the Institute of Remote Sensing Application, Chinese Academy of Sciences, Beijing 100101, China.

M. R. Caetano is with the National Centre for Geographic Information (CNIG), Lisbon, Portugal.

Publisher Item Identifier S 0196-2892(99)01979-8.

$t_{ff}(h)$ Hemispherical-hemispherical path transmittance for a horizontally homogeneous plant canopy with thickness h.

$t_{df}(h,\theta_i)$ Directional-hemispherical path transmittance for a horizontally homogeneous plant canopy with thickness h and incident angle θ_i.

$t_o(h,\theta_i)$ Direct transmittance for a horizontally homogeneous plant canopy with thickness h and incident angle θ_i.

$t'_{ff}(h)$ Hemispherical-hemispherical path transmittance for a discontinuous plant canopy with thickness h.

$t'_{df}(h,\theta_i)$ Directional-hemispherical path transmittance for a discontinuous plant canopy with thickness h and at incident angle θ_i.

$t'_o(h,\theta_i)$ Direct transmittance without any scattering for a discontinuous plant canopy with thickness h and at incident angle θ_i.

$T^{\infty}_{df}(\theta_i)$ Directional hemispherical path transmittance for a semi-infinite horizontally homogeneous medium at incident angle θ_i.

T^{∞}_{ff} Hemispherical hemispherical path transmittance of a semi-infinite horizontally homogeneous medium.

t_L Leaf transmittance.

$T(\theta_i)$ Signature of shaded crown surface.

$Z(\theta_i)$ Signature of shaded background.

Greek:

γ $\sqrt{1-\omega}$, $\omega = t_L + r_L$.

θ_i Illumination zenith angle.

θ'_i Illumination zenith angle in the transformed dimension.

θ_v Viewing zenith angle.

θ'_v Viewing zenith angle in the transformed dimension.

λ Crown count density (m^{-2}).

μ_i $\cos(\theta_i)$.

μ_v $\cos(\theta_v)$.

ξ Angle between incident and viewing directions.

$\rho_{ff}(h)$ Hemispherical–hemispherical path reflectance for a horizontally homogeneous plant canopy with thickness h.

$\rho_{df}(h,\theta_i)$ Directional-hemispherical path reflectance for a horizontally homogeneous plant canopy with thickness h andat incident angle θ_i.

$\rho'_{ff}(h)$ Hemispherical–hemispherical path reflectance for a discontinuous plant canopy with thickness h.

$\rho'_{df}(h,\theta_i)$ Directional-hemispherical path reflectance for a discontinuous plant canopy with thickness h and at incident angle θ_i.

$\tau(\theta_i)$ Projected foliage area volume density at direction θ_i (m^{-1}).

ϕ Relative azimuth angle between illumination and viewing directions.

ω Single scattering albedo.

I. Introduction

VEGETATED land surfaces scatter radiation anisotropically in many wavelengths. The bidirectional reflectance distribution function (BRDF) [1] specifies the behavior of scattering over the vegetated land surface as a function of illumination and viewing angles and land surface parameters. Modeling the BRDF provides an improved understanding of the physical processes of light interaction with vegetation canopies and further has the practical benefit of allowing improved interpretation of remote sensing data. Following the launch of the Moderate Resolution Imaging Spectroradiometer (MODIS) and Multi-angle Imaging Spectroradiometer (MISR) sensors by NASA's Earth Observing System (EOS), inversion of BRDF models has great potential to provide the surface parameters needed for climate and vegetation studies from remotely sensed data.

There are numerous BRDF models to describe the anisotropic reflectance of vegetation, including empirical functions [2], semiempirical functions [3], [4] and physical models. The physical models include radiative transfer (RT) [5] and geometric optics (GO) [6]–[9], or combined RT and GO [10], ray tracing [11], [12] and radiosity model [13], [14]. Each approach has specific advantages and disadvantages, depending on the particular applications for which they were designed, which are summarized in several recent reviews [15]–[18].

All models have to deal with the interactions of light occurring within and between individual plant canopies. There are two basic physical processes involved. The first such process is the surface scattering effect, also known as hotspot effect, the opposition effect or the geometric effect. The scene objects, such as leaves, stems and trunks and crowns that comprise the plant canopy cast shadows on other plants and the background. The primary cause of the hotspot in most vegetation canopies is the absence of shadows observable from the direction of illumination. However, in vegetation with large numbers of wavelength-sized structures, such as mosses, the hotspot is dominated by an interference phenomenon, so called coherent backscatter [23]. For complex canopies which include leaves, stems, trunks, and crowns, due to clumping of leaves, the hotspot due to shadow-hiding includes effects from multiple levels. Usually the smaller the ratio of the object size to the distance between the objects is, the sharper the hotspot [19]. The second primary effect is multiple scattering among leaves, crowns, and background, which is best handled using radiative transfer theory.

Radiative transfer theory was developed to describe photon transfer within a horizontally homogeneous layer of media, such as the atmosphere, or also dense vegetation canopies. Usually numerical methods are used to solve the complicated radiative transfer equation, but other analytical approxima-

tions of radiative transfer theory have advantages. Hapke [20] developed a BRDF model for a homogeneous semi-infinite media composed of uniformly distributed scatterers. In his model, the singly scattered radiance is derived exactly, whereas the multiply scattered radiance is evaluated from a two-stream approximation, assuming that the scatterers comprising the canopy are isotropic. Verstraete *et al.* [21] followed Hapke's model to develop a BRDF model for homogeneous semi-infinite plant canopies by accounting explicitly for the effects of leaf orientation and geometrical arrangement in the canopy, or the hotspot effect. These models have shown great advantages in inversion [22]. But in reality, the canopy layer usually can not consider as a semi-infinite layer, so the application of Hapke's model is difficult. Usually in remote sensing of vegetation, the radiance is modeled by using unscattered radiance, single scattering radiance and multiple scattered radiance. The first two terms are modeled exactly and the multiple scattering is calculated from the two stream approximation analytically [24]–[26]. The explicit analytical model by Qin and Jupp [26] also considers the effect of angular distribution of canopy leaf surfaces. They found that the leaf shape and orientation have a considerable influence on the canopy hotspot except for planophile canopies or in near nadir viewing directions. The contributions from soil reflectance and multiple scattering increase with the modal inclination angles of leaves. More recently, Qin and Xiang [27] used their analytical model to model the effect of all foliage elements and their possibly nonrandom dispersion in space on directional reflectance, they found that the canopy hotspot becomes strongest when the mean inclination angle of foliage elements is around 20°, then it rapidly decreases with an increase in that angle.

For discontinuous plant canopies, tree crowns cast shadows on trees and the background, which strongly conditions the brightness of the vegetation cover as seen from a given viewpoint in the hemisphere. This led to the development of the geometric optical (GO) models ([6]–[9]). In GO models, the scene is treated as an assemblage of three dimensional tree crowns with specific shape and size. The scene as viewed by a sensor includes four components: sunlit crown, shaded crown, sunlit background, and shaded background. The bidirectional reflectance is modeled as a linear combination of four component spectral signatures, weighted by their areal proportions, which in turn are modeled as functions of the shape and size of tree crowns, their count densities and illumination and viewing directions.

One question associated with using GO models concerns the estimation of the component spectral signatures. One approach has been to measure them in the field, which was used effectively to estimate the BRDF of forests in Maine [28]. However, measuring these component spectral signatures can be difficult due to the requirement for measurements above the canopy. An alternative approach is to estimate component signatures based on analysis of image data, which has been done for forests in Oregon [29] and California [30]. The problem with this approach is that it is entirely empirical. The GO model is simple, which has advantages for surface parameter retrievals [31], [32]. But the necessity to provide the component spectral signatures has undermined application of the GO models.

The component spectral signatures are the result of multiple scattering based on radiative transfer. More recently, Li *et al.* [10] developed a hybrid GORT model, which combines the geometric optics of large scale canopy structure with principles of radiative transfer for volume scattering within individual crowns. While single scattering and light penetration have been modeled accurately, the assumption of uniform multiple scattering from the sunlit and shaded surfaces of crowns has limited the estimation of the bidirectional reflectance [10].

This study explores a simple but still physically-based hybrid GO and RT model for estimating the BRDF's of discrete plant canopies, such as forests, woodlands, savannas, or shrublands. To develop this simple hybrid BRDF model for discontinuous plant canopies, the basic structure of the geometric optical model is followed, but the analytical approximations of radiative transfer for a horizontally homogeneous medium with a finite thickness derived in [33] are used to model the reflectance of the components.

Clumping of leaves into branches and branches into crowns leads to shadowing effects at multiple scale. The original GO model only includes shadowing effects at the crown level [9]. In this study, a finer-level hotspot function is also included in the reflectance calculation of the sunlit crown component. This result thus forms an analytical hybrid GORT-BRDF model as an alternative to Li *et al.*'s more complicated numerical GORT-BRDF model [10].

II. Background

Radiation interaction with a plant canopy is affected by many factors, including the source distribution (proportions of incident beam irradiance and diffuse skylight, and its spectral properties), the canopy structure, as well as the spectral properties of the canopy elements and the canopy background and illumination and viewing geometry. The proportions of beam irradiance and diffuse skylight and its spectral properties depend on atmospheric conditions and waveband. Due to high absorption by plants in the visible wavelengths (0.4–0.7 μm), radiation interception approaches absorption and multiple scattering is very small [34]. Due to the high leaf albedo in the near infrared, multiple scattering within the canopy layer and between the ground surface and the canopy are greater.

A complete description of a canopy structure requires the specification of the position, size, and orientation of each element in the canopy, which has proven to be complicated and impractical. Usually statistical parameters of canopy structure, such as the leaf area index (LAI), leaf angle distribution (LAD) and the spatial arrangement of canopy foliage, branches, and stems are used in mathematical models.

The effect of LAI and LAD on the radiation regime for horizontally homogeneous plant canopies is well developed (see the review in [15]). The canopy gap probability (or Beer's law) was first used by Monsi and Saeki [35] to describe the beam penetration. The gap probability was defined as the probability that a beam misses a set of randomly located leaves.

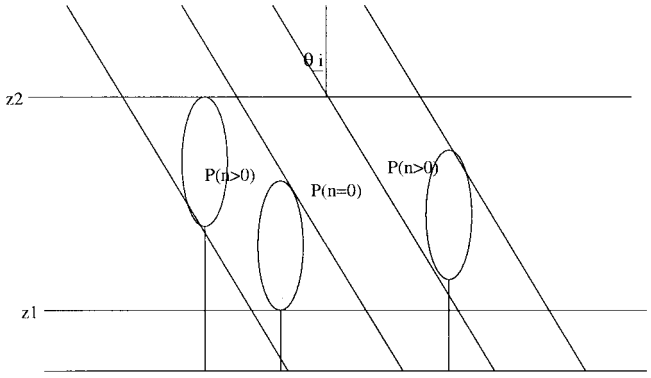

Fig. 1. Between-crown and within-crown gap probabilities; n indicates the number of crowns that light passes through.

The clumping of canopy leaves into crowns for discontinuous plant canopies results in a nearly horizontally homogeneous distribution of canopy elements within crowns. Small canopy gaps within the crowns (or within-crown gaps) and the larger canopy canopy gaps between crowns (or between-crown gaps) exist for discontinuous plant canopies. No attenuation will occur when light passes through the between-crown gaps, and the proportion of the directly transmitted light passing through the within-crown gaps will obey Beer's Law, which is an exponential function of the total within-crown path length. Gap probabilities are critical when modeling solar radiation interaction within discontinuous plant canopies [10], [36].

A. Between- and Within-Crown Gap Probabilities for Discontinuous Plant Canopies

There are two types of gap probabilities for discontinuous plant canopies: the between-crown gap probability and the within-crown gap probability (see Fig. 1). The between-crown gap probability $P(n = 0|h, \theta_i)$ for direct beam radiation describes the proportion of the direct solar beam at solar zenith angle θ_i that reaches a point at a depth h within the plant canopies without passing through any crowns (i.e., $n = 0$). The within-crown gap probability $P(n > 0|h, \theta_i)$ is defined as the proportion of direct beam radiation passing through at least one crown (n is the number of crowns) without being scattered. The theory for calculating both of these gap probabilities has been developed by Li *et al.* [10]. The between-crown gap probability is modeled based on Boolean set theory, i.e. an exponential function of crown number within the beam projected cylinder volume with a radius r starting from the top of the canopy layer to depth h. The within-crown gap probability is described by Beer's Law, but its calculation is rather complicated since the within-crown path length is a random variable. The location where a beam enters a crown, the number of crowns through which it passes and the pathlength through an individual crown are random. So in order to calculate the within-crown path length, the distribution of numbers of crowns intercepted by a beam and within-crown pathlength distribution have to be modeled first based on some statistical features of the Possion distribution. The calculation is rather complicated and the details can be found in [10], [36].

To illustrate the difference in gap probabilities for homogeneous and discontinuous plant canopies, Fig. 2 shows the vertical distribution of the gap probability (of an old jack pine forest in central Canada) predicted by GORT model for discontinuous plant canopies and Beer's Law for the homogeneous case at different solar zenith angles. This figure shows that the vertical distribution of gap probabilities for discontinuous plant canopies resembles a logistic curve of sigmoidal shape as a function of height, with most of the radiation intercepted in middle of the canopy, whereas for homogeneous plant canopies, the predictions from Beer's Law are simply exponential functions. The cause of the deviation from an exponential function like Beer's Law is the between-crown gap probability. A second effect is that at larger solar zenith angles, the gap probabilities for the two different plant canopies become similar.

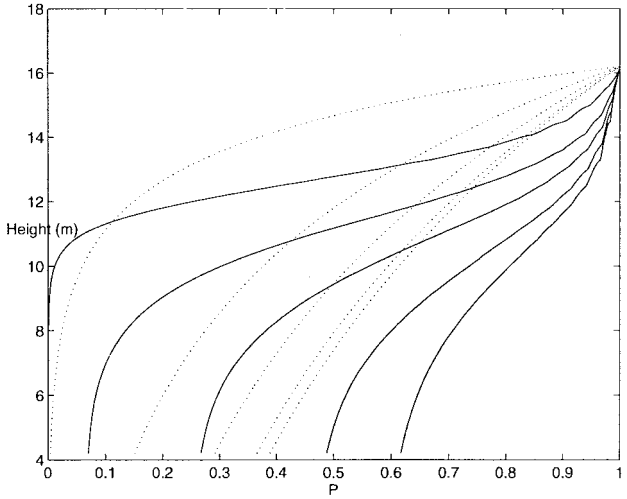

Fig. 2. Comparison of gap probabilities in an old jack pine forest in central Canada as predicted by the GORT model and Beer's Law for a variety of solar zenith angles.

The gap probability for diffuse skylight, or the "openness factor," K_{open} is the integral of the gap probability for direct beams over the hemisphere. It includes the between-crown openness factor $K_{\text{open}}(n = 0)$, which is the integral of the between-crown gap probability over the hemisphere. The within-crown openness factor $K_{\text{open}}(n > 0)$ is the integral of the within-crown gap probability over the hemisphere.

The between-crown and within-crown gap probabilities for discontinuous plant canopies allows us to model the effect of complex canopy structure on the radiation environment with the canopies. The work by Ni *et al.* [36] also showed the effect of the horizontal whorl structure on the radiation transmission over boreal forests by incorporating the horizontal whorl structure on gap probabilities.

B. Bidirectional Within-Crown Gap Probability

To model the bidirectional within-crown gap probability, Kuusk's bidirectional within-crown gap probability for a single tree is used [37], [38]:

$$P(n > 0|h, \theta_i, \theta_v, \phi) = e^{-\tau(\theta_i) l_i(h,\theta_i)} e^{-\tau(\theta_v) l_v(h,\theta_v)} \cdot e^{\tau(\theta_i)\sqrt{l_i(h,\theta_i) l_v(h,\theta_v)} \frac{(1-e^{-k_l l_{iv}}}{k_l l_{iv})}} \quad (1)$$

where $\tau(\theta_i)$ is the extinction coefficient with unit $(1/m)$, $k_l = (1/s_l)$, where s_l is the characteristic linear dimension of foliage elements, $l_i(h,\theta_i)$ and $l_v(h,\theta_v)$ are the within-crown path lengths within a single crown at incident angle θ_i and viewing angle θ_v, and

$$l_{i,v}(h,\theta_i,\theta_v) = \sqrt{l_i^2 + l_v^2 - 2l_i l_v \cos\xi}. \tag{2}$$

In (1), the first term $e^{-\tau(\theta_i)l_i(h,\theta_i)}$ and the second term $e^{-\tau(\theta_v)l_v(h,\theta_v)}$ are the gap probabilities within a single crown at zenith angle θ_i and θ_v individually, and the last part is the hotspot function, i.e.,

$$H(n>0|h,\theta_i,\theta_v,\phi) = e^{\tau(\theta_i)\sqrt{l_i(h,\theta_i)l_v(h,\theta_v)}\left(1.0-e^{-k_l l_{iv}/k_l l_{iv}}\right)}. \tag{3}$$

To apply this to all crowns, i.e., the light passing through not only one crown, but more than one crown as well, we take full use of the within-crown gap probability for discontinuous plant canopies, $P(n>0|h,\theta_i)$ and $P(n>0|h,\theta_v)$. The bidirectional within-crown gap probability for discontinuous plant canopies can be calculated as

$$P(n>0|h,\theta_i,\theta_v,\phi) = P(n>0|h,\theta_i)P(n>0|h,\theta_v)H(n>0|h,\theta_i,\theta_v,\phi) \tag{4}$$

where the formula of $H(n>0|\theta_i,\theta_v,\phi)$ is the same as described above: $k_l = (1/s_l), s_l$ is the horizontal crown radius, l_i, l_v, l_{iv} are calculated based on the within-crown gap probabilities, as described above:

$$l_i(h,\theta_i) = \frac{-\ln(P(n>0|h,\theta_i))}{\tau(\theta_i)} \tag{5}$$

$$l_v(h,\theta_v) = \frac{-\ln(P(n>0|h,\theta_v))}{\tau(\theta_v)} \tag{6}$$

$$l_{i,v}(h,\theta_i,\theta_v) = \sqrt{l_i^2 + l_v^2 - 2l_i l_v\ \cos\xi}. \tag{7}$$

Note that $P(n>0|h,\theta_i)$ and $P(n>0|h,\theta_v)$ are the within-crown gap probabilities at solar zenith angle, θ_i and viewing zenith angle, θ_v, which are calculated based on the tree geometry parameters, and $P(n>0|h,\theta_i,\theta_v,\phi)$ is the bidirectional within-crown gap probability calculated based on (4).

C. Multiple Scattering Within Discontinuous Plant Canopies

Numerical solutions for radiative transfer are complicated and hence simpler solutions are desirable. As an improvement, with the two stream approximation, using doubling and adding method, the analytical solution for radiative transfer for a horizontally homogeneous canopy layer with finite thickness was derived in [33]. Define $t_{df}(h,\theta_i)$ as the directional-hemispherical transmittance, $t_{ff}(h)$ as hemispherical-hemispherical transmittance, $\rho_{df}(h,\theta_i)$ as directional-hemispherical reflectance, and $\rho_{ff}(h)$ as the hemispherical-hemispherical reflectance, where h is the thickness of the horizontally homogeneous canopy layer, and θ_i is the incident zenith angle, then

$$t_{ff}(h) = T_{ff}^{\infty}(h)\ \frac{1-(R_{ff}^{\infty})^2}{1-(T_{ff}^{\infty}(h)R_{ff}^{\infty})^2} \tag{8}$$

$$\rho_{ff}(h) = R_{ff}^{\infty}\ \frac{1-(T_{ff}^{\infty}(h))^2}{1-(T_{ff}^{\infty}(h)R_{ff}^{\infty})^2} \tag{9}$$

$$t_{df}(h,\theta_i) = T_{df}^{\infty}(h,\theta_i) - \rho_{ff}(h)[t_0(h,\theta_i)R_{df}^{\infty}(\theta_i) + T_{df}^{\infty}(h,\theta_i)R_{ff}^{\infty}] \tag{10}$$

$$\rho_{df}(h,\theta_i) = R_{df}^{\infty}(\theta_i) - t_{ff}(h)[t_0(h,\theta_i)R_{df}^{\infty}(\theta_i) + T_{df}^{\infty}(h,\theta_i)R_{ff}^{\infty}] \tag{11}$$

where $R_{ff}^{\infty}, R_{df}^{\infty}(\theta_i), T_{ff}^{\infty}(h)$, and $T_{df}^{\infty}(h,\theta_i)$ are directional-hemispherical reflectance, hemispherical–hemispherical reflectance, directional-hemispherical transmittance, and hemispherical-hemispherical transmittance for a semi-infinite homogeneous layer, respectively, which are

$$R_{ff}^{\infty} = \frac{1-\gamma}{1+\gamma}$$

$$R_{df}^{\infty}(\theta_i) = \frac{1-\gamma}{1+2\mu_i\gamma}$$

$$T_{ff}^{\infty}(h) = e^{-2\gamma\tau h,}$$

$$T_{df}^{\infty}(h,\theta_i) = \frac{\omega}{2}\ \frac{1+2\mu_i}{1-(2\gamma\mu_i)^2}[T_{ff}^{\infty}(h) - t_0(h,\theta_i)]$$

where

$\gamma = \sqrt{1-\omega}, \omega$	is the single scattering albedo of a canopy element;
$t_0(h,\theta_i) = e^{-(\tau(\theta_i)h/\mu_i)}$	unscattered transmittance;
$\mu_i = \cos(\theta_i)$	extinction coefficient for a plant canopy layer;
τ	$k(\theta_i)\cdot$ FAVD;
$k(\theta_i)$	fraction of the foliage area projected toward the incident zenith angle θ_i;
FAVD	foliage area volume density.

To apply the analytical approximation of radiative transfer for a homogeneous layer to discontinuous plant canopies, an approach is employed which has the effect of squeezing all the plants together and leaving all the gaps (between-crown gaps and within-crown gaps) together. Then the whole canopy can be divided into a homogeneous vegetation layer and a layer without vegetation. The canopy elements are assumed homogeneously distributed in space within the vegetation layer, and the transmittance and reflectance for light passing through the vegetation layer will be estimated by the analytical solutions of the path scattering parameters for a horizontally homogeneous layer. The light passing through the layer without vegetation will remain unattenuated. The scattering parameters for the discontinuous plant canopy can be approximated by the analytical solution of radiative transfer and gap probabilities, i.e,

$$t_o'(h,\theta_i) = P(n=0|h,\theta_i) + P(n>0|h,\theta_i) \tag{12}$$

$$t_{df}'(h,\theta_i) = t_{df}(h,\theta_i)(1-t_o'(h,\theta_i)) \tag{13}$$

$$t_{ff}' = t_{ff}(1.0 - K_{\text{open}}) + K_{\text{open}} \tag{14}$$

$$\rho'_{df}(h,\theta_i) = \rho_{df}(h,\theta_i) \tag{15}$$

$$\rho'_{ff}(h) = \rho_{ff}(h) \tag{16}$$

where

- K_{open} $= K_{\text{open}}(n=0) + K_{\text{open}}(n>0)$;
- $t'_o(h,\theta_i)$ direct transmittance without any scattering for a discontinuous plant canopy with thickness h and incident angle θ_i;
- $t'_{ff}(h)$ hemispherical–hemispherical path transmittance for a discontinuous plant canopy with thickness h;
- $\rho'_{ff}(h)$ hemispherical–hemispherical path reflectance for a discontinuous plant canopy with thickness h;
- $t'_{df}(h,\theta_i)$ directional-hemispherical path transmittance for a discontinuous plant canopy with thickness h and incident angle θ_i;
- $\rho'_{df}(h,\theta_i)$ directional-hemispherical path reflectance for a discontinuous plant canopy with thickness h and incident angle θ_i.

III. An Analytical Bidirectional Reflectance Model

In the GO model, the forest canopy is treated as an assemblage of discrete tree crowns with specific shape and size. The scene has four components, sunlit crowns, shaded crowns, sunlit background, shaded background (Fig. 3). The bidirectional reflectance of the scene as a whole is modeled as the sum of radiances or reflectances of individual components as weighted by their areal proportions, i.e.,

$$R(\theta_i,\theta_v,\phi) = K_c C + K_g G + K_t T + K_z Z \tag{17}$$

where

- θ_i, θ_v solar zenith and viewing zenith angles;
- ϕ relative azimuth angle;
- K_c areal proportion of sunlit and viewed crown;
- K_g areal proportion of the sunlit and viewed background;
- K_t areal proportion of shaded and viewed crown;
- K_z areal proportion of shaded and viewed background.

The quantities K_c, K_g, K_z, and K_t are well modeled as functions of tree geometry and sun and viewing geometry based on the principles of geometric optics as described by Li and Strahler [9]. In this study, the spectral signatures of the four components, C, G, T, or Z, are modeled based on the analytical approximation of scattering parameters for discontinuous plant canopies described above. The finer level hotspot, such as the hotspot by leaf, branch and trunk, will also be included in the spectral signature of sunlit crown based on the bidirectional within-crown gap probability. Using this approach, the model captures the multi-level hotspot effect for discontinuous plant canopies, and also the multiple scattering based on radiative transfer.

A. Areal Proportions of the Four Components

The Li–Strahler geometric optical mutual shadowing (GOMS) model [9] is used to estimate the areal proportions of the four components. The GOMS model is a modified version of their previous model [7] to accommodate more properly the effects of mutual shadowing of individual plant crowns, which are taken as geometric objects that cast shadows on the background and on other crowns. When the crowns are closely spaced and of similar size, the shadow of one crown tends to fall preferentially on the base of an adjacent crown. Thus when the canopy is viewed from a low angle, only the sunlit tops of crowns are seen. This effect gives the BRDF a bowl-shape when plotted in a hemispherical projection.

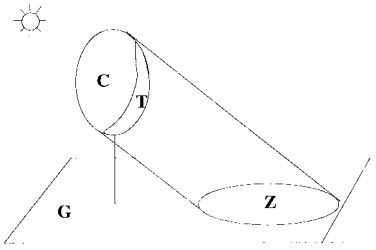

Fig. 3. The four scene components used in the geometric optical model: C is sunlit tree crown, T is shaded tree crown, G is sunlit background, and Z is shaded background.

In the GOMS model, the areal proportions of the sunlit crowns and sunlit background are calculated as functions of the tree crown size, density, and the illumination and viewing directions, but the shaded tree crowns and background are treated as a single component. Here they are separated as follows:

$$K_z = e^{-(\lambda\pi r^2/\cos(\theta'_v))} - K_g \tag{18}$$

$$K_t = 1.0 - K_c - K_z - K_g \tag{19}$$

where $\theta'_v = tan^{-1}((b/r)\ \tan(\theta_v))$ (19)

B. Spectral Signatures of the Four Components

The reflectance of a sunlit crown varies as a function of canopy depth. This leads to less brightness near the edges of the crown and increased brightness near the center. The spectral signature of other components may not be uniform either. But for natural vegetation, the variation between signatures of the sunlit and shaded crowns and background is generally much greater than the variation within signatures of these components. So in this study the nonuniformity of component signatures due to multiple scattering effects is neglected.

The spectral signatures C, G, T, and Z are defined as the brightness of the sunlit crown, sunlit background, shaded crown and shaded background. The incoming radiation usually includes direct beam and diffuse skylight, as a result the component signatures are the results of two terms from direct beam and diffuse skylight:

$$C = f_d C_d + (1-f_d) C_f \tag{20}$$

$$T = f_d T_d + (1-f_d) T_f \tag{21}$$

$$G = f_d G_d + (1-f_d) G_f \tag{22}$$

$$Z = f_d Z_d + (1-f_d) Z_f \tag{23}$$

where f_d is the proportion of incident direct beam, and the quantities C_d, T_d, Z_d are the contributions by the direct beam;

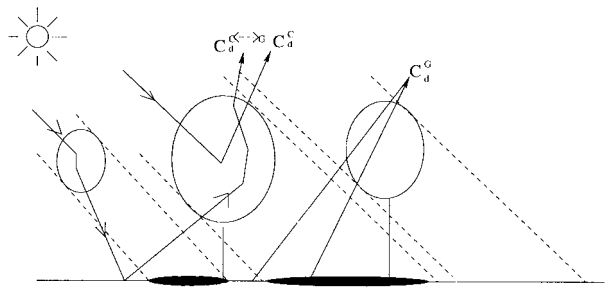

Fig. 4. The signature of sunlit crown component $C_d = C_d^C + C_d^G + C_d^{C\langle - \rangle G}$.

C_f, T_f, Z_f are the contributions by the diffuse skylight to the component signatures. The spectral signature of each component will be addressed as follows.

- G_d and G_f: For the time being, the background is simply assumed to be Lambertian. This simple assumption is not a problem for denser vegetation. In future studies, the bidirectional effect of background reflectance can be added as needed when applied to very sparse canopy. G_d and G_f are simply modeled as background albedo.

$$G_d = \rho_s \tag{24}$$
$$G_f = \rho_s. \tag{25}$$

- Z_d and Z_f: For simplification, these two terms are modeled by the light scattered and directly passing through the within-crown gaps and reflected by the background, i.e.

$$Z_d = (t'_{df} + P(\theta_i | n > 0))\rho_s \tag{26}$$
$$Z_f = (t'_{ff} - K_{\text{open}}(n > 0))\rho_s. \tag{27}$$

- C_d and C_f are composed of three components (see Fig. 4):

$$C_d = C_d^C + C_d^G + C_d^{C\langle - \rangle G} \tag{28}$$
$$C_f = C_f^C + C_f^G + C_f^{C\langle - \rangle G}. \tag{29}$$

C_d^C and C_f^C are the path reflectances over crowns, i.e., the incident direct and diffuse radiation scattered within crowns. As defined earlier, the signature of the components are assumed Lambertian. But due to effect of self-shadowing of canopy elements within crowns, such as leaves, branches, this also leads to brighter sunlit crown at backward scattering. Here we assume the surface of sunlit crown is partly Lambertian and partly non-Lambertian, The Lambertian part is modeled by ρ'_{df} and $\rho'_{ff}(h)$. The non-Lambertian part are caused by the finer level hotspot, which is modeled by the bidirectional within-crown gap probability based on the modified formulas of Kuusk's hotspot model [38], i.e. $p(n > 0|\theta_i, \theta_v, \phi)\omega(1-g)/2\mu_i\mu_v$, by adding the asymmetry effect of scattering, where g is the phase function asymmetry factor, and $g = -(4/9)(r_L - t_L/\omega)$ [15]. Since the non-Lambertian function is contributed by the first scattering function, we put a factor $(1-\omega)$ in the hotspot function, i.e., $(1-\omega)p(n > 0|\theta_i, \theta_v, \phi)\omega(1-g)/2\mu_i\mu_v$:

$$C_d^C = \rho'_{df} + \frac{(1-\omega)p(n > 0|\theta_i, \theta_v, \phi)\omega(1-g)}{2\mu_i\mu_v} \tag{30}$$
$$C_f^C = \rho'_{ff}(h). \tag{31}$$

Notice that the hotspot function is ignored in C_f^C.

C_d^G and C_f^G are the first-order scattered radiance from soil. The viewer sees the background through the within-crown gaps of the canopy. C_d^G and C_f^G are the contributions from the background. The background is partly sunlit and partly shadowed. When the viewer is in coincidence with the sun position, the viewer sees the sunlit background, otherwise more shaded background will be seen. With the knowledge of reflectance of sunlit background and shaded background, the brightness of the nonviewable background is the linear combination of sunlit background and shaded background, i.e., $ZK'_z + GK'_g$, where K'_z and K'_g are the shaded background and sunlit background and nonviewable to the viewer:

$$K'_g = e^{-(\lambda\pi r^2/\cos(\theta'_i))} - K_g \tag{32}$$
$$K'_z = (1 - e^{-(\lambda\pi r^2/\cos(\theta'_v))}) - K'_g \tag{33}$$

where $\theta'_i = \tan^{-1}((b/r)\ \tan(\theta_i))$ and $\theta'_v = \tan^{-1}((b/r)\ \tan(\theta_v))$. The first term in (33), $e^{-(\lambda\pi r^2/\cos(\theta'_i))}$, is the areal proportion of sunlit background including viewed and nonviewable, K_g is the areal proportion of sunlit and viewed background. The first term in (33), $1 - e^{-(\lambda\pi r^2/\cos(\theta'_v))}$, is the areal proportion of nonviewable background including sunlit and viewed background. The viewer sees the background through the within-crown gaps, C_d^G and C_f^G are expressed as

$$C_d^G = (ZK'_z + GK'_g)\, K_{\text{open}}(n > 0) \tag{34}$$
$$C_f^G = (K_{\text{open}}G + (1 - K_{\text{open}})Z)\, K_{\text{open}}(n > 0). \tag{35}$$

$C_d^{C\langle - \rangle G}$ and $C_f^{C\langle - \rangle G}$ are the multiple scattering between the canopy layer and the background. A proportion of the incoming photons flux will pass through the canopy layer and be scattered by the background surface. These photons may be scattered back and forth between the canopy layer and the background surface until they escape from the canopy layer or are absorbed by the canopy elements or the background surface. The successive reflections back and forth between the canopy layer and background surface occurs in a geometric (doubling) manner. This amount of scattered radiance is modeled as

$$C_d^{C\langle - \rangle G} = (t'_{df} + t'_o)\ \frac{\rho_s}{1.0 - \rho_s\rho'_{ff}}\ (t'_{ff} - K_{\text{open}}(n = 0)) \tag{36}$$
$$C_f^{C\langle - \rangle G} = t'_{ff}\ \frac{\rho_s}{1.0 - \rho_s\rho'_{ff}}\ (t'_{ff} - K_{\text{open}}(n = 0)). \tag{37}$$

- Fourth, T_d and T_f are the brightness of shaded and viewed crowns. For simplification, these two terms are

modeled by the light scattered back and forward between the background and the canopy layer, i.e.,

$$T_d = (t'_{df} + t'_o)\,\frac{\rho_s}{1.0 - \rho_s \rho'_{ff}}\,(t'_{ff} - K_{\text{open}}(n=0)) \tag{38}$$

$$T_f = t'_{ff}\,\frac{\rho_s}{1.0 - \rho_s \rho'_{ff}}\,(t'_{ff} - K_{\text{open}}(n=0)). \tag{39}$$

Notice that the component terms C and T are also affected by the neighboring crowns. This factor is usually small and very complicated to model, we ignore it here.

By tracking the multiple scattering within crowns and the scattering between canopy layer and background, they are modeled as functions of the analytical approximation of scattering parameters as described above and background albedo. The finer level hotspot, such as the hotspot by leaf, branch and trunk, is included in the spectral signature of sunlit crown through bidirectional within-crown gap probability. Using this approach, the model captures the multi-level hotspot effect for discontinuous plant canopies, and also the multiple scattering based on radiative transfer. The geometric optical model captures the mutual shadowing effect at crown level, and the finer level hotspot function captures the mutual shadowing effect at finer canopy structure level, such as leaf, branch, and trunk.

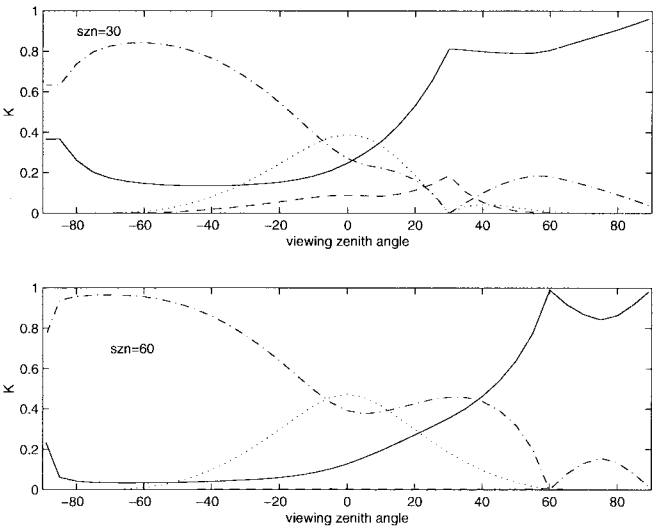

Fig. 5. Modeled areal proportions of four components in the SOBS site based on geometric optics. 1) Sunlit and viewed background, K_g (dash line): peak value at hotspot and local peak at nadir; note that K_g is frequently close to zero at solar zenith angle 60° and thus difficult to see; 2) sunlit and viewed crown surface, K_c (solid line): a bowl shape with a peak at hotspot—crown level hotspot; 3) shaded and viewed crown, K_t (dash-dot line): a sine wave with local minimum at nadir and zero at hotspot; 4) shaded and viewed background, K_z (dot line): a peak value at nadir and zero at hotspot. Sharper hotspot indicating stronger shadowing effect with the increase of solar zenith angle.

IV. Model Predictions and Comparisons with Field Measurements

The Boreal Ecosystem Atmosphere Study (BOREAS) has been conducted in Canada since 1992 [41]. Its purpose is to improve process models which describe the exchanges of energy, water, carbon, and trace constituents between the boreal forest and the atmosphere, and to develop methods for applying the process models over large spatial scales using remote sensing and other integrative modeling techniques.

During the intensive field campaigns of the BOREAS experiment, several instruments were used to collect multiangular measurements. POLDER (POLarization and Directionality of Earth Reflectances) and ASAS (Advanced Solid-State Array Spectroradiometer) were installed on the C-130 aircraft operated by NASA Ames Research Center, and POLDER was also installed on the helicopter provided by NASA Wallops Flight Facility, respectively. Both instruments measure hyperspectral and multiangle bidirectional reflectance over the land surface. During the field campaigns, the aircraft or the helicopter flew over the "flux tower sites," where tree geometry parameters had been measured, providing the opportunities to validate our model.

ASAS is an airborne imaging spectroradiometer that was modified to point off-nadir by NASA/GSFC for the purpose of remotely observing directional anisotropy of solar radiance reflected from terrestrial surfaces. The instrument is capable of pointing from approximately 70° from zenith forward to 55° aft along-track (in the direction of flight). For BOREAS data collection flights, ASAS collected imagery at most flux tower sites at eight different view zenith angles: +70, +60, +45, +26, nadir, −26, −45, −55°. ASAS data were acquired in 62 spectral bands ranging from 404 to 1023 nm with a spectral resolution of approximately 10 nm in each band [45].

POLDER is an optical sensor designed to observe the surface reflectance in visible and near infrared bands. It operates on a framing camera that acquires multiple overlapping frames along the flight pass. In this way, locations within the flight pass are observed from many different viewpoints. POLDER has a wide field-of-view lens with ±51° along the track and ±3° cross track, and a CCD array detector to collect images [46], [47].

Like the ASAS instrument, the directional signature measured by the POLDER instrument is derived from multiple measurements acquired from various positions. The difference is that ASAS acquires measurements for specific viewing angles whereas POLDER makes many, near-instantaneous multidirectional measurements. The resulting angular resolution for POLDER depends on the aircraft speed relative to its altitude and the position of the location with respect to the center of the flight line. The major weakness of the POLDER instrument, for the measurement of angular signatures, is its limitation to viewing angles of less than 60°. In particular, it is difficult to fully analyze the hot spot when the solar zenith angle is larger than about 50°.

Also, PARABOLA (Portable Apparatus for Rapid Acquisition [48] of Bidirectional Observations of the Land and Atmosphere) measurements were acquired from a movable platform supported by a 70 m dual steel cable tramway at more than 10 m above the flux tower sites.

Each of the above instruments has merits and drawbacks for the purpose of validating the new BRDF model. Due to the large field of view (15°), PARABOLA measurements are dispersed and the hot spot is not as clearly measured

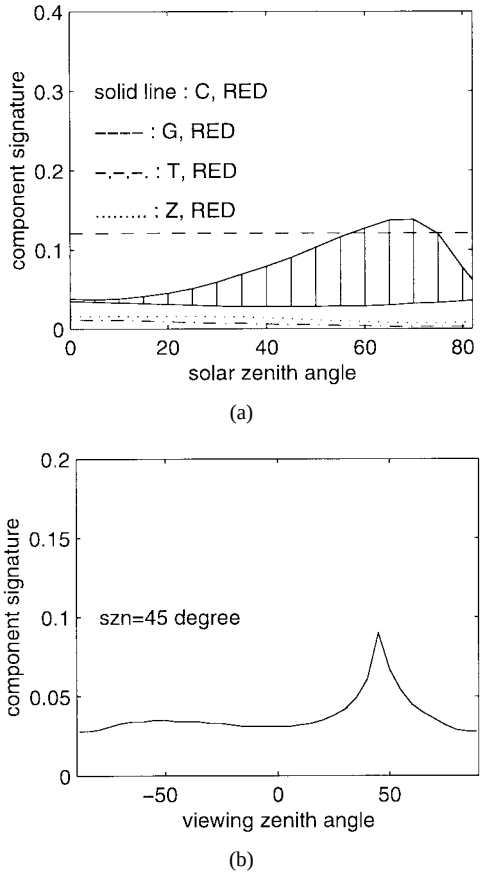

Fig. 6. Calculated component signatures in visible spectrum as a function of solar zenith angle (top) and C at solar zenith angle $= 45°$ as a function of viewing zenith angle (bottom) in the SOBS site. The vertical bars between the lines of C in the top plot shows the value of C at specific solar zenith angles for a range of viewing directions. The line for C in the bottom plot shows an extension of the vertical bar at solar zenith angle $= 45°$.

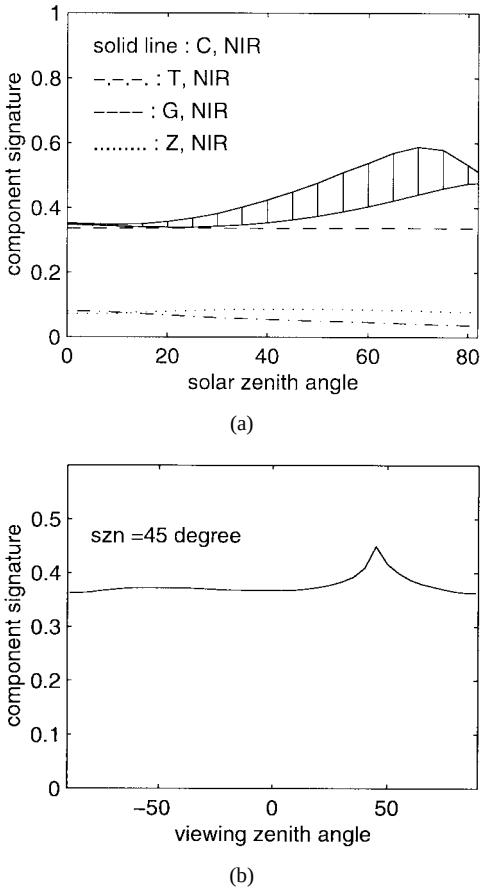

Fig. 7. The same as Fig. 6 except for the near infrared.

as in the ASAS and POLDER measurements. On the other hand, at large viewing zenith angles, the ASAS images are badly distorted. For POLDER instruments, the largest viewing zenith angle is only 60°. So both ASAS and POLDER measurements do not obtain very good measurements at large viewing zenith angles. PARABOLA, however, does have large viewing angles. So model validation was performed by using measurements from all three instruments.

TABLE I
INPUT TREE PARAMETER VALUES FOR GORT

Site	$R(m)$	$b(m)$	$\lambda(\frac{1}{m^2})$	$h_1(m)$	$h_2(m)$	$FAVD(\frac{1}{m^2})$
SOBS	0.76	2.7	0.41	3.0	8.5	0.858

TABLE II
SPECTRAL PROPERTIES OF CANOPY AND SOIL BACKGROUND

	Leaf transmittance	Leaf reflectance	Background albedo
540 nm	0.06	0.2	0.069
670 nm	0.002	0.09	0.29
865 nm	0.305	0.515	0.29

A. Model Prediction

From the GO model, the areal proportions of the four components are modeled as functions of the tree geometry parameters, such as the tree size, height, density, sun and viewing geometry. The component spectral signatures are modeled as functions of the tree geometry parameters, leaf area index, sun and viewing geometry (for calculation of gap probabilities) and spectral properties of the canopy elements and background surface (for calculation of the scattering parameters). The input parameters for the model are as follows.

1) Sun and viewing zenith angles.
2) Tree geometry parameters (the vertical and horizontal crown radii, r, b, and crown count density, λ, lower and upper boundary of crown center, h_1 and h_2.
3) Foliage area volume density (FAVD).
4) Leaf transmittance and reflectance,, t_1 r_L.

To illustrate the properties of the areal proportion and component signature terms, Fig. 5 shows the modeled areal proportions of the four components in the principal plane, which is the plane defined by the direction of illumination and the normal to the surface, for the Old Black Spruce stand in the Southern Study Area of BOREAS (called the SOBS site). Figs. 6 and 7 show the modeled spectral signatures of the four components in the visible and near infrared. The input parameters for this model are shown in Tables I and II. The value of the background albedo is from measurements by Miller *et al.* [42], the values of leaf transmittances and reflectances are from the measurements by Middleton and

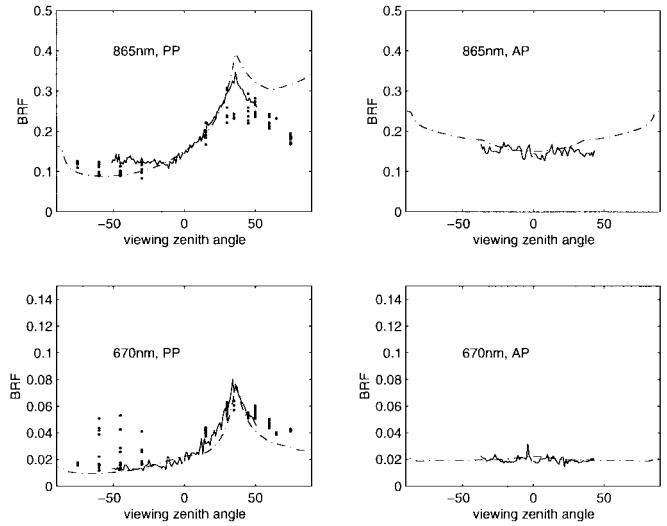

Fig. 8. Comparison of the modeled (dash-dot line) bidirectional reflectance factor (BRF) in principal plane (left) and across the principal plane (right) in the red (670 nm) (bottom) and near infrared (865 nm) (top) with POLDER measurements (solid line) and PARABOLA measurements (dots) in the old black spruce forest in the southern site (SOBS) of BOREAS in 1994. The solar zenith angle is 36°.

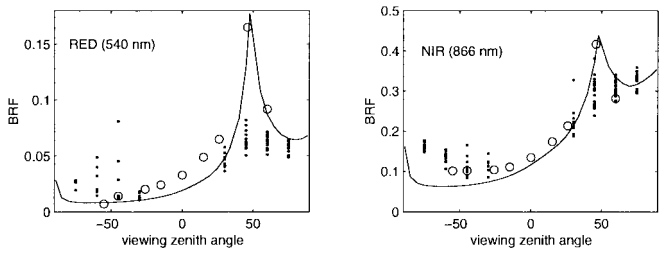

Fig. 9. Comparison of the modeled (solid line) bidirectional reflectance factor (BRF) in the principal plane in the red spectral range (540 nm) (left) and near-infrared (866 nm) with ASAS (circles) and PARABOLA measurements (dots) in the old black spruce forest in the southern site (SOBS) of BOREAS in 1994. The solar zenith angle is 47.7°.

Walter-Shea [43], and the rest are from Ni *et al.* [36]. The beam proportion, $f_d(\mu_i) = \frac{\mu_i}{0.09+\mu_i}$ for clear days is from field measurements [36].

Fig. 5 shows the patterns of the areal proportion of the four components as a function of solar zenith and viewing angles. The areal proportion of sunlit background K_g with the change of viewing direction shows a peak value at the hotspot viewing direction. The fraction of sunlit crown K_c as a function of viewing direction exhibits a bowl shape, and a maximum value at the the hotspot. The shape of the shaded crown proportion K_t is like a sine wave with a local minimum value at the nadir and becomes zero at the hotspot. The shaded background K_z shows a peak value at nadir and is zero at the hotspot direction. The above patterns of the four components explain the shadowing effect of tree crowns well. At the hotspot, no shadows are observable, so no shaded crown and shaded background can be seen and the sunlit crown and sunlit background are at peak values. At the nadir viewing direction, more lower canopy or background can be seen, thus the shaded background reaches a maximum value and the sunlit background reaches a local peak value. Fig. 5 also shows the sunlit crown with a sharper hotspot as solar zenith angle increases. This indicates that the shadowing effect is stronger with increasing solar zenith angle.

Figs. 6 and 7 show that the spectral signature of sunlit crown C is a function of both solar zenith angle and viewing zenith angle. The value of C increases with solar zenith angles (see the top plots in Figs. 6 and 7) and has a maximum value at the hotspot viewing direction (see the bottom plots in Figs. 6 and 7) due to the shadowing effect from finer structures such as branches, trunks and leaves. The spectral signature of sunlit background G is approximated by the background albedo, and constant with the change of sun and viewing directions. The signatures of shaded crown T and background Z are modeled as functions of solar zenith angle, but are almost constant. In both the visible and near infrared, G and C are comparable, with much larger values than the shaded terms T and Z. The comparable values of G and C in visible and near infrared implies that the background includes considerable vegetation.

B. Comparison of Model Results With Field Measurements

Figs. 8 and 9 show the comparison of the modeled bidirectional reflectance with the PARABOLA, POLDER and ASAS measurements in the SOBS site. POLDER provides many finer angular measurements for the changing of viewing directions, so they are plotted as a line. ASAS has only measurements at only a few viewing angles, and they are plotted as circles. Both ASAS and POLDER measurements show a stronger hotspot than the PARABOLA measurements, as previously explained.

The PARABOLA is a sphere-scanning radiometer with a a conical field of view of 15°. Given this move of operation, the PARABOLA measurements at each viewing direction exhibit variation due to the variation in observed proportions of the scene components at the various points sampled in the stand. Second, due to the width of the field of view, PARABOLA measurements do not show a strong hotspot compared with the ASAS and POLDER measurements.

Fig. 8 shows that the model predictions fit the POLDER and PARABOLA measurements well in the principal plane and across the principal plane in both visible and near infrared spectral ranges at a solar zenith angle of 36° except for slight overestimation of field measurements in the backward scattering after hotspot angle. Fig. 9 shows for a solar zenith angle of 47.7° that the model fits well with the ASAS and PARABOLA measurements in visible and near infrared in the principal plane.

The comparison of the model results with POLDER, ASAS, and PARABOLA measurements indicates that the model captures the features of the bidirectional reflectances over conifer forests in the principal plane and across the principal plane in the visible and near infrared. Slight overestimation of POLDER measurement after hotspot angle in near infrared is still under investigation.

In the principal plane, the basic feature of the bidirectional reflectance over discontinuous plant canopies is a bowl shape with a strong hotspot at backward scattering. As indicated in Fig. 5, the areal proportion of sunlit crown as a function of viewing direction is a bowl shape with a peak value at the hotspot angle. Since the sunlit crown is bright compared

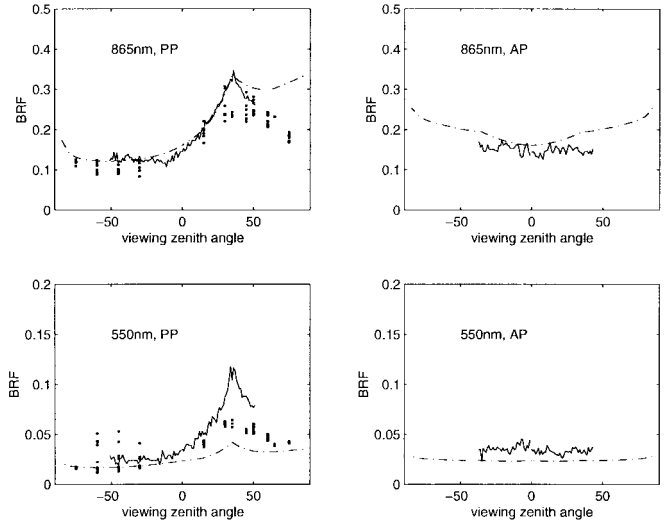

Fig. 10. Comparison of the modeled (dash-dot line) (using the model without the multiscale hotspot function) bidirectional reflectance factor (BRF) in the principal plane (left) and across the principal plane (right) in the red (550 nm) (bottom) and near infrared (865 nm) (top) with POLDER measurement (solid line) and PARABOLA measurements (dots) in the old black spruce forest in the southern site (SOBS) of BOREAS in 1994. The solar zenith angle is 36°.

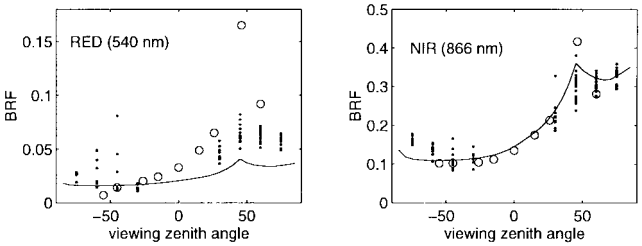

Fig. 11. Comparison of the modeled (solid line) (using the model without the multiscale hotspot function) bidirectional reflectance factor (BRF) in the principal plane in the red spectral range (540 nm) (left) and near-infrared (866 nm) with ASAS (circles) and PARABOLA measurements (dots) in the old black spruce forest in the southern site (SOBS) of BOREAS in 1994. The solar zenith angle is 47.7°.

to the other components, the sunlit crown dominates the shape of BRDF over discontinuous plant canopies. But the shape of the areal proportion of sunlit crown is only a measure of the hotspot at the crown level. Figs. 10 and 11 show the comparison of the modeled results using the hybrid GORT model without considering the finer level hotspot with POLDER, ASAS, and PARABOLA measurements [44]. For these predictions of this hybrid GORT model by Ni *et al.* [44], the spectral signatures of the four components are modeled as functions of solar zenith angle but are constant with the viewing zenith angle. It is not like the new model developed here which models the spectral signatures as a function of solar zenith angle and viewing zenith angle as well. Figs. 10 and 11 show that the model without the finer level hotspot function models reasonably well with POLDER, ASAS and PARABOLA measurements in near infrared but underestimates the measurements at hotspot in visible. This is understandable because the hotspot is stronger in visible than near infrared due to much higher light absorption by green leaves in the visible than in the near infrared.

A multiscale hotspot exists for conifer forests. The study by Ni *et al.* [36] shows the hierarchical clumping including the clumping of needles into shoots, shoots into branches, branches into whorls, and whorls into crowns, with crowns comprising the canopy. When the sun and the viewing directions are the same, the shadowing effect of branches, trunks, stems, shoots, or needles results in the increase of the reflectance, which leads to a brighter sunlit crown at hotspot angle than other viewing directions. Prior research has shown that the width of the hotspot is related to ratio of size and distance between objects [19]. The ratio is related to the the size and density of scene objects. Due to the differences of the size and density of crowns, stems, branches, shoots, or needles for conifer forests, multiscale hotspots overlap each other. Comparison of the shape of areal proportion of sunlit crown (only shows crown-level hotspot) with that of the multiangular reflectance measurements (ASAS, POLDER) or the model predictions as functions of viewing direction, indicates that the later are sharper. This demonstrates that the hotspot effects over discontinuous plant canopies are caused by hotspot effects at multiple scales.

As discussed earlier, the gap probabilities including between-crown and within-crown gap probabilities for discontinuous plant canopies are a measure of the hierarchical canopy structure, the effect of whorl orientation of conifer forest on radiation transmission can be well modeled through gap probabilities [36]. In this study, the effect of the whorl orientation on canopy reflectance was also modeled through gap probability.

In this study, the multiscale hotspot function is developed based on the gap probabilities for discontinuous plant canopies. This is the reason that the new model presented here captures the feature of multiscale hotspot for discontinuous plant canopies.

V. Discussion and Conclusions

This study presents a simple hybrid geometric optical and radiative transfer (GORT) approach to model the effect of canopy structure on bidirectional reflectance. This hybrid model has advantages relative to either pure RT or pure GO approaches. Pure GO models can capture the basic structure of discontinuous plant canopies, i.e., the clumping of leaves into crowns, which cast shadows; thus, the area covered by the field of view of sensors is a mixture of sunlit and shaded crowns and background. Combined with this approach, the analytical approximation of radiative transfer was used to model the multiple scattering within crowns between leaves. The RT approach accounts for the influence of the optical properties of the foliage on multiple scattering. Gap probabilities play a crucial rule in the application of radiative transfer for discontinuous plant canopies and in deriving the finer level hotspot functions.

This study provides an analytical hybrid GORT model compared to Li *et al.*'s original version for the bidirectional reflectance over discontinuous plant canopies [10] in the following aspects. First, Li *et al.*'s original GORT model assumes uniform multiple scattering from the sunlit and shaded crown surfaces. Model validation with measurements in a conifer stand in Howland, Maine showed that the assumption is

not appropriate for discontinuous plant canopies, and multiple scattering is higher from the sunlit crown surface [10]. The current version overcomes this problem by modeling the spectral signatures of the sunlit crown and shaded crown separately. By considering the path scattering effect on the sunlit crown, the modeled sunlit crown is brighter than the shaded crown. Second, an analytical approximation of the radiative transfer equation is used instead of the numerical method in the original GORT model so that the component signatures can be calculated by a few simple formulae. Using this approach the bidirectional reflectance over discontinuous plant canopies was modeled as a function of the solar and viewing geometry, the tree geometry parameters and the spectral properties (single scattering albedo) of the canopy elements and the background. Third, finer level hotspot caused by shadowing effect at leaf and branch level are well modeled here.

Model validation with multiple angular measurements in a boreal conifer stand shows that the model captures the main features of the bidirectional reflectance over discontinuous plant canopies, including the bowl shape with the change of viewing direction and the hotspot effect. Slight overestimation of POLDER measurements at backward scattering after hotspot angle is still under investigation.

This model has been validated over dense forests. Future work will involve the validation of the model for very sparse canopies, such as woodlands, savanna, etc. The anisotropic effect of the background will be added if necessary.

ACKNOWLEDGMENT

The authors acknowledge M. Leroy and P. Bicheron (CESBIO, Toulouse, France), F.-M. Breón (LMCE, Saclay, France) for providing the POLDER data, J. R. Irons for providing ASAS data, and Dr. D. W. Deering, for the PARABOLA data. Constructive comments from anonymous reviewers were appreciated and incorporated into the final manuscript. Valuable disscussion with W. Qin also contributed to the improvement of this manuscript. Special thanks to G. Meister for his critical reading on this manuscript.

REFERENCES

[1] F. E. Nicodemus, J. C. Richmond, J. J. Hsia, E. I. Ginsberg, and T. Limperis, "Geometrical considerations and nomenclature for reflectance," *NBS Monograph*, no. 160, Inst. Basic Stand., Washington, D.C., 1977.

[2] C. L. Walthall, J. M. Norman, J. M. Welles, G. Campbell, and B. L. Bald, "Simple equation to approximate the bidirectional reflectance from vegetation canopies and bare soil surfaces," *Appl. Opt.*, vol. 24, pp. 383–387, 1985.

[3] J. L. Roujean, M. Leroy, and P.-Y. Deschamps, "A bidirectional reflectance model of the earth's surface for the correction of remote sensing data," *J. Geophys. Res.*, vol. D18, pp. 20455–20468, 1992.

[4] W. Wanner, X. Li, and A. H. Strahler, "On the derivation of kernels for kernel-driven models of bidirectional reflectance," *J. Geophys. Res.*, vol. D10, pp. 21077–21089, 1995.

[5] R. B. Myneni, G. Asrar, and F. G. Hall, "A three-dimensional radiative transfer method for optical remote sensing of vegetated land surfaces," *Remote Sens. Environ.*, vol. 41, pp. 105–121, 1992.

[6] X. Li and A. H. Strahler, "Geometric-optical modeling of a coniferous forest canopy," *IEEE Trans. Geosci. Remote Sensing*, vol. GE-23, pp. 207–221, 1985.

[7] ——, "Geometric-optical bidirectional reflectance modeling of a coniferous forest canopy," *IEEE Trans. Geosci. Remote Sensing*, vol. GE-24, pp. 281–293, 1986.

[8] A. H. Strahler and D. L. B. Jupp, "Modeling bidirectional reflectance of forests and woodlands using Boolean models and geometric optics," *Remote Sens. Environ.*, vol. 34, pp. 153–160, 1990.

[9] X. Li and A. H. Strahler, "Geometric-optical bidirectional reflectance modeling of discrete crown vegetation canopy: Effect of crown shape and mutual shadowing," *IEEE Trans. Geosci. Remote Sensing*, vol. 30, pp. 276–292, Mar. 1992.

[10] X. Li, A. H. Strahler, and C. E. Woodcock, "A hybrid geometric optical-radiative transfer approach for modeling albedo and directional reflectance of discontinuous canopies," *IEEE Trans. Geosci. Remote Sensing*, vol. 33, pp. 466–480, 1995.

[11] D. S. Kimes and J. A. Kirchner, "Radiative transfer model for heterogeneous 3-D scenes," *Appl. Opt.*, vol. 21, pp. 4119–4129, 1982.

[12] J. K. Ross and A. Marshak, "Monte Carlo methods," in *Photon-Vegetation Interactions—Application in Optical Remote Sensing and Plant Ecology*, R. B. Myneni and J. Ross, Eds. Berlin, Germany: Springer-Verlag, 1991.

[13] S. A. W. Gerstl and C. C. Borel, "Principles of the radiosity method versus radiative transfer for canopy reflectance modeling," *IEEE Trans. Geosci. Remote Sensing*, vol. 30, pp. 271–274, 1992.

[14] N. S. Goel, I. Rozehnal, and R. L. Thompson, "A computer graphics based model for scattering from objects of arbitrary shapes in the optical region," *Remote Sens. Rev.*, vol. 36, pp. 73–104, 1991.

[15] J. K. Ross, *The Radiation Regime and Aarchitecture of Plant Sstands*. The Hague, The Netherlands: W. Junk, 1981, p. 391.

[16] ——, "Models of vegetation canopy reflectance and their use in estimation of biophysical parameters from reflectance data," *Remote Sens. Rev.*, vol. 4, pp. 1–212, 1988.

[17] R. B. Myneni, J. K. Ross, and G. Asrar, "A review on the theory of photon transport in leaf canopies in a slab geometry," *Agric. Forest Meteorol.*, vol. 45, pp. 1–153, 1990.

[18] A. H. Strahler, "Vegetation canopy reflectance modeling—recent developments and remote sensing perspectives," *Remote Sens. Rev.*, vol. 15, pp. 179–194, 1997.

[19] B. Hapke, D. DiMucci, R. Nelson, and W. Smythe, "The cause of the hot spot in vegetation canopies and soils: Shadow-hiding versus coherent backscatter," *Remote Sens. Environ.*, vol. 58, pp. 63–68, 1996.

[20] D. L. B. Jupp and A.H. Strahler, "A hotspot model for leaf canopies," *Remote Sens. Environ.*, vol. 38, pp. 193–210, 1991.

[21] B. Hapke, "Bidirectional reflectance spectroscopy," *J. Geophys. Res.*, vol. 86, no. B4, P3039–3054, 1981.

[22] M. M. Verstraete, B. Pinty, and R. E. Dickinson, "A physical model of the bidirectional reflectance of vegetation canopies 1. Theory," *J. Geophys. Res.*, vol. 95, pp. 11 755–11 765, 1990.

[23] B. Pinty, M. M. Verstraete, and R. E. Dickinson, "A physical model of the bidirectional reflectance of vegetation canopies 2. Inversion and validation," *J. Geophys. Res.*, vol. 95, pp. 11 767–11 775, 1990.

[24] T. Nilson, "Approximate analytical methods for calculating the reflection functions of leaf canopies in remote sensing applications," *Photon-Vegetation Interactions—Application in Optical Remote Sensing and Plant Ecology*, R. B. Myneni and J. Ross, Eds. Berlin, Germany: Springer-Verlag, 1991, pp. 162–189.

[25] W. Qin, "Modeling bidirectional reflectances of multicomponent vegetation canopies," *Remote Sens. Environ.*, vol. 46, pp. 235–245, 1993.

[26] W. Qin and D. L. B. Jupp, "An analytical and computationally efficient reflectance model for leaf canopies," *Agric. Forest Meteorol.*, vol. 66, pp. 31–64, 1993.

[27] W. Qin and Y. Xiang, "An analytical model for bidirectional reflectances factor of multicomponent vegetation canopies," *Sci. China*, vol. 40, pp. 305–315, 1997

[28] C. Schaaf and A. H. Strahler, "Validation of bidirectional and hemispherical reflectance from a geometric-optical model using ASAS imagery and pyranometer measurements of a spruce forest," *Remote Sens. Environ.*, vol. 49, pp. 138–144, 1994.

[29] W. Wu and A. H. Strahler, "Remote estimation of crown size, stand density and foliage biomass on the Oregon transect," *Ecol. Appl.*, vol. 4, pp. 299–312.

[30] C. E. Woodcock, J. B. Collins, V. D. Jakabhazy, X. Li, and S. A. Macomber, "Inversion of the Li-Strahler model for mapping forest structure," *IEEE Trans. Geosci. Remote Sensing*, vol. 35, pp. 405–414, Mar. 1997.

[31] C. E. Woodcock, J. B. Collins, S. Gopal, C. D. Jakahazy, X. Li, S. Macomber, S. Ryherd, Y. Wu, V. J. Harward, J. Levitan, and R. Warbinton, "Mapping forest vegetation using Landsat TM imagery and a canopy reflectance model," *Remote Sens. Environ.*, vol. 50, pp. 240–254, 1994.

[32] X. Li and A. H. Strahler, "A knowledge-based inversion of physical BRDF models and three case studies," in *Proc. Int. Geosci. Remote Sensing Symp.*, 1996, pp. 2173–2175.
[33] W. Ni, X. Li, and C. E. Woodcock "Analytical approximation of radiative transfer for a finite horizontally homogeneous plant canopies," submitted for publication.
[34] J. L. Roujean, "A tractable physical model of shortwave radiation interception by vegetation canopies," *J. Geophys. Res.*, vol. 101, pp. 9523–9532, 1996.
[35] M. Monsi and T. Saeki, "Über den lichtfaktor in den pflanzengesellschaften und seine bedeutung für die stoffproduction," *Jpn. J. Botany*, vol. 14, pp. 22–52, 1953,
[36] W. Ni, X. Li, C. E. Woodcock, J. L. Roujean, and R. Davis, "Transmission of solar radiation in boreal conifer forests: Measurements and models," *J. Geophys. Res.*, vol. 102, no. D24, pp. 29 555–29 566, 1997.
[37] A. E. Kuusk, "Scattering of direct solar radiation in the crown of an isolated tree," *Earth Res. Space*, vol. 2, pp. 1-6-111, 1987 (in Russian) [Engl. transl. in *Sov. K. Remote Sens*].
[38] ———, "The hotspot effect in plant canopy reflectance," *Photon-Vegetation Interactions—Application in Optical Remote Sensing and Plant Ecology*, R. B. Myneni and J. Ross, Eds. Berlin, Germany: Springer-Verlag, 1991, pp. 140–159.
[39] S. Chandrasekhar, *Radiative Transfer*. New York: Dover, 1960.
[40] J. Hansen and L. Travis, "Light scattering in planetary atmospheres," *Space Sci. Rev.*, 1974.
[41] P. J. Sellers, F. G. Hall, H. Margolis, B. Kelly, D. Baldocchi, J. den Hartog, J. Cihlar, M. Ryan, B. Goodison, P. Crill, J. Ranson, D. Lettenmaier, and D. E. Wickland, " The Boreal ecosystem-atmosphere Study (BOREAS): An overview and early results from the 1994 field year," *Bull. Amer. Meteorol. Soc.*, vol. 76, pp. 1549–1577, 1995.
[42] J. R. Miller, H. P. White, J. M. Chen, D. R. Peddle, G. McDermid, R. A. Foumier, P. Shepherd, I. Rubinstein, J. Freemantle, R. Soffer, and E. LeDrew, "Seasonal change in understory reflectance of boreal forests and influence on canopy vegetation indices," *J. Geophys. Res.*, vol. 102, no. D24, pp. 29 729–29 736, 1997.
[43] E. M. Middleton and E. A. Walter-Shea, "Optical properties of canopy elements in the boreal forest," in *Proc. Int. Geosci. Remote Sensing Symp.*, 1995, pp. 789–793.
[44] W. Ni, X. Li, C. E. Woodcock, and A. Strahler, "Parameterization of spectral component signatures for geometric optical canopy reflectance modeling," *J. Remote Sensing*, vol. 1, (suppl. 1), pp. 108–111, 1997.
[45] J. R. Irons, K. J. Ranson, D. L. Williams, R. R. Irish, and F. G. Huegel, "An off-nadir pointing imaging Spectroradiometer for terrestrial ecosystem studies," *IEEE Trans. Geosci. Remote Sensing*, vol. 29, pp. 66–74, Jan. 1991.
[46] P. Y. Deschamps, F. M. Breón, M. Leroy, A. Podaire, A. Bricaud, J. C. Buriez, and G. Sèze, "The POLDER mission: Instrument characteristics and scientific objectives," *IEEE Trans. Geosci. Remote Sensing*, vol. 32, pp. 598–615, 1994.
[47] F. M. Breón, V. Vanderbilt, M. Leroy, P. Bicheron, C. L. Walthall, and J. E. Kalshoven, "Evidence of hot spot directional signature from airborne POLDER measurements," *IEEE Trans. Geosci. Remote Sensing*, vol. 35, pp. 479–484, 1997.
[48] D. W. Deering and P. Leone, "A sphere scanning radiometer for rapid directional measurements of sky and ground radiance," *Remote Sens. Environ.*, vol. 19, pp. 1–24, 1986.

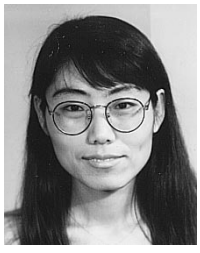

Wenge Ni (M'98) received the B.S. in meteorology from Nanjing Institute of Meteorology, nanjing, China, in 1988, the M.S. in micrometeorology from the Department of Natural Resource Management and Engineering, The University of Connecticut, Storrs, in 1994, and the Ph.D. degree in remote sensing from the Department of Geography, Boston University, Boston, MA, 1997.

She has been with Raytheon STX (formerly Hughes STX), Lanham, MD, since 1997, working as a Principal Scientist on the algorithm design of the retrieval of global albedo retrieval from the Visible/Infrared Imager/Radiometer Suite (VIIRS) of the National Polar-orbiting Operational Environmental Satellite System (NPOESS). Her current research interests include the theory and application of bidirectional reflectance over vegetation, the spatial variance analysis of remote sensing images, and the study of energy balance over vegetated land surfaces.

Xiaowen Li graduated from the Chengdu Institute of Radio Engineering, China, in 1968. He received the M.A. degree in geography and the M.S. degree in electrical and computer engineering, both in 1981, and the Ph.D. degree in geography in 1985, all from the University of California, Santa Barbara.

He is now a Professor at the Institute of Remote Sensing Application, Chinese Academy of Science, Beijing, China. He is also a Research Professor at the Center of Remote Sensing and the Department of Geography, Boston University, Boston, MA. His primary research interests are in 3-D modeling of reflectance and thermal emission of land surface, vegetation in particular, and information extraction from mutiangular remote sensed images.

Curtis E. Woodcock (M'90) received the B.A., M.A., and Ph.D. degrees from the Department of Geography, University of California, Santa Barbara.

Since 1984, he has taught at Boston University, Boston, MA, where he is currently Associate Professor and Chair of Geography and a Resercher in the Center for Remote Sensing. His primary research interests in remote sensing include mapping and inventory of forests and other natural environments, spatial modeling of images and inversion of reflectance models, and image processing and geographic information systems. He is also interested in the detection of environmental change using remote sensing.

Dr. Woodcock is a member of the American Society of Photogrammetry and Remote Sensing.

Mário R. Caetano received the Forest Engineering degree from Lisbon University of Technology, Lisbon, Portugal, in 1989 and the M.A. degree in geography from the University of California, Santa Barbara, in 1995.

He is currently a Researcher at the National Centre for Goegraphic Information (CNIG), Lisbon, working methodology development for application of remotely sensed data resources management. He is also responsible for the development of the Earth Observation National Network.

Alan H. Strahler (M'86), for a photograph and biography, see this issue, p. 738.